



Research article

Subcutaneous injection of hyaluronic acid leading to embolism and recanalization process monitored in real time by three-dimensional photoacoustic imaging

Fengbing He^{a,1}, Xingzhi Luo^{b,1}, Fan Meng^a, Jiarui Chen^a, Chao hao Liang^a, Yiqing Zhang^a, Shutong Liu^a, Zishan Yuan^a, Wuyu Zhang^b, Yanping He^{a,**}, Jian Zhang^{a,*}

^a Qingyuan People's Hospital, The Sixth Affiliated Hospital of Guangzhou Medical University, School of Biomedical Engineering, Guangzhou Medical University, Guangdong, China

^b MOE Key Laboratory of Laser Life Science & Institute of Laser Life Science, College of Biophotonics, South China Normal University, Guangzhou, China

ARTICLE INFO

Keywords:

Photoacoustic imaging
Filler injection
Hyaluronic acid
Vascular compromise

ABSTRACT

This study describes a method for real-time examination of the microvascular system based on the three-dimensional photoacoustic imaging system to prevent arterial complications, especially vascular embolism, during hyaluronic acid (HA) injections. Chicken embryos were used to simulate the superficial blood vessels of human skin, and then the target area was imaged by the photoacoustic imaging system for three-dimensional vascular imaging, and then the syringe and blood vessels were monitored, and the syringe angle and penetration depth were adjusted in time using an injection device to avoid puncturing the arterial vasculature and clogging the blood vessels. HA was then injected into smaller vessels on the dorsum of the tongue in mice and into thicker vessels on the dorsal portion of the tongue in rats to mimic embolization, and the post-operative recovery was reflected by the changes in the pixel dots of the extracted part of the blocked blood vessels, and it was observed that the blood flow in the area of the fine vessels was restored in about 3 days, whereas blood flow in the area of the large vessels was restored in only about 1 h. The method presented in this paper allows precise guidance of injectable filler HA, which has good application prospects in improving the safety of injection micro-plastic surgery and reducing the experience requirements for medical personnel.

1. Introduction

Cosmetic plastic surgery is the surgical method of altering an individual's appearance for the purpose of beautifying or improving specific areas or correcting birth defects [1,2]. According to the American Society for Aesthetic Plastic Surgery, up to 80.9 % of cosmetic minimally invasive surgical injections in recent years have focused on facial fillers and shaping, these injectable procedures

* Corresponding author.

** Corresponding author.

E-mail addresses: hyp052001@aliyun.com (Y. He), jianzhang@gzhmu.edu.cn (J. Zhang).

¹ These authors contributed equally to this study.

typically use hyaluronic acid (HA) and Botox as injectable materials [3,4]. HA is a transparent, gel-like substance consisting of a polymer with a repeating arrangement of N-acetylglucosamine groups and D-glucuronic acid, which has important physiological functions in the body, including smoothing the skin, speeding up wound healing, relieving joint pain and preventing bladder pain [5]. In cosmetic applications, the main thing is to help the skin maintain moisture, smoothing fine lines, moisturising depressed areas and lifting the contours of the face, and its operation is less painful, the effect is significant, more and more widely accepted by candidates, so it is the most common method of facial rejuvenation treatment [6–8]. For intradermal injection, the needle should be inserted into the skin with the bevelled side up and at an angle of 5° to the skin. For subcutaneous injection, the needle should be inserted into the skin at an angle of 30–40°. However, HA injection requires the operator to have systematic anatomical knowledge, rich injection experience and rigorous attitude, but today's medical cosmetic practitioners have different technical levels, resulting in more and more complications after HA injection [9,10].

Incorrect injection techniques can cause significant damage. Inexperience in injecting fillers can lead to uneven distribution of fillers in the skin, which can produce cosmetic results contrary to expectations [11,12]. When injecting fillers, if the needle damages the blood vessel wall, this can lead to extravasation of blood, causing hematomas and petechiae [13]. If HA injections are too close to the skin surface, a blue translucent line resembling a bruise may appear (Tyndall effect) [14]. The most serious consequence is the possibility of vascular embolism. This usually occurs when HA is injected into a blood vessel, resulting in the formation of a thrombus or embolism and interruption of the normal blood supply to the vessel, with subsequent development of ulceration or necrosis at the injection site [15–17]. If the filler is injected into an artery and causes a reversal of blood flow near the bifurcation of the central retinal artery, the filler will advance with the blood flow and eventually form a blockage, resulting in loss of vision [18–20].

In current clinical practice, the detection of HA injection-related embolism is mainly done by observing whether the patient develops abnormal symptoms after the injection, such as local pain, swelling and other signs, and by performing blood tests and coagulation function tests [21–23]. There are also effective tests such as ultrasound, computer tomography and magnetic resonance imaging, which can help doctors monitor the blood flow and diagnose whether a clot has formed [24–26]. However, these methods may not be intuitive enough or require a large investment of medical resources, or may be invasive and pose hidden risks to patients.

In this study, we propose a method for guiding HA injections through an assisted injection device based on a three-dimensional (3D) photoacoustic imaging (PAI) system, with the aim of reducing the risk of HA injections are providing convenient post-injection imaging. We were able to guide the injector needle through the 3D PAI system to avoid the vascular veins of the chick embryo model, and to achieve continuous observation of HA occlusion of small and large blood vessels and blood flow recovery. These applications can help cosmetic surgeons to perform HA injections more accurately and reduce the risk of vascular occlusion from a preventive perspective.

2. Materials and methods

2.1. Animals and ethics statement

All experimental protocols involving animals were conducted under the Guidelines for Institutional Animal Care and Use

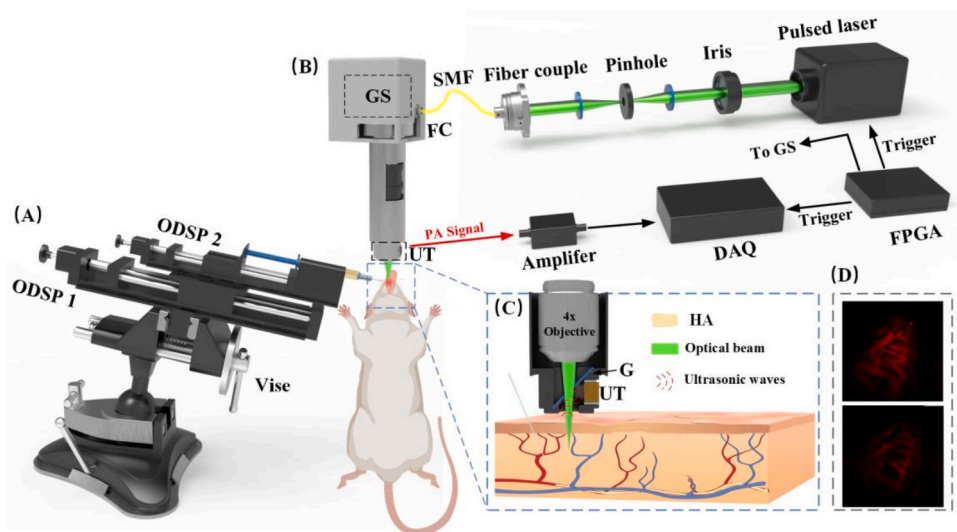


Fig. 1. Schematic diagram of a hand-held photoacoustic imaging system. (A) Components of the assisted injection device. (B) Composition of the PAI system. (C) Enlarged cross-sectional view of the blue dashed box. (D) The PAI of normal vascular and the PAI after HA filler. ODSP, one-dimensional sliding platforms; GS, galvanometer scanner; FC, fiber collimator; SMF, signal-mode fiber; DAQ, data acquisition; FPGA, field-programmable gate array; G, glass; UT, ultrasonic transducer. (For interpretation of the references to colour in this figure legend, the reader is referred to the Web version of this article.)

Committee and approved by the Animal Care and Use Committee of Guangdong Zhiyuan Biomedical Technology Co., Ltd (IAEC-2022011202). The KM mice and the SD rats used in the experiments were obtained from Beijing Vitasin Biotechnology Co. Eight-week-old KM mice and SD rats were selected for this study. All animals were quarantined prior to the experiment and no common infectious pathogens were found. At the end of the experiment, the experimental animals will be euthanized, cervical dislocation for KM mice and carbon dioxide inhalation for rats. The HA (Colena, Korea) is provided by Qingyuan People's Hospital in Guangdong Province, China and it was made from sterile, pyrogen-free, highly purified HA gel of non-animal origin, which is a filler macromolecule, and was supplemented with 0.3 % lidocaine to reduce pain.

2.2. Hand-held PAI system

The conventional PAI system has some limitations, such as the need for a large spatial extent and the difficulty of mobility. In this study, the coupled optical fiber technology and the drive-controlled galvanometer scanning method are used to achieve a miniaturised PAI device, which can then be more easily used in various scenarios [27,28]. The imaging system used in this study as illustrated in Fig. 1. Since the 532 nm laser matches the absorption peaks of haemoglobin, it can be effectively absorbed by haemoglobin, producing a strong photoacoustic signal. This property gives the 532 nm laser an advantage in detecting signal integrity within blood vessels and can be used to determine the presence of thrombus formation. By detecting the intensity and characteristics of the photoacoustic signal, an abnormal photoacoustic response can be observed within the blood vessel to identify and assess the presence and status of intravascular thrombus.

A laser (Mosquito X 532-2-V, InnoLas) produces a pulsed laser with 532 nm wavelength and a frequency of 50 kHz. The laser beam is coupled into a fiber via a fiber coupler (PAF2-7A, Thorlabs) for better control and flexibility and then collimated to ensure parallel propagation. The laser was transmitted through the fiber to a fiber collimator (F240FC-532, Thorlabs) and passed through a two-dimensional galvanometer scanner (SS9107, Sunny Technology) which allows precise scanning or positioning of the laser beam. The laser beam is then directed to a 4× flat field objective (RMS4, Thorlabs). The photoacoustic signals generated by the laser interaction with the sample are then collected and detected by a 15 MHz ultrasound transducer (manufactured by Guangdong Photoacoustic Technology Co., Ltd.). And a glass plate is positioned at an angle of 45° to the transducer and reflects the photoacoustic signals towards it. The collected ultrasonic signals were amplified using a 50 dB low noise amplifier (PA-650L, Guangdong Photoacoustic Technology Co., Ltd.) and transferred to a computer equipped with a data acquisition module (M4i, 4450-x8, Spectrum) and an image processing module for further analysis. The biaxial galvanometer was controlled by an FPGA for 2D scanning. Due to light exit limitations, the final imaging area was a circular area of 5 mm diameter. The pulsed laser illumination energy of 12 mJ/cm² at 532 nm was less than the ANSI safety limit [29]. The experimental procedure was performed with water as the coupling medium, which was enclosed in the probe by a transparent film to prevent the generation of air leakage that could affect the imaging quality.

2.3. Assisted injection device

In HA filler procedures, the classic method is to insert the needle at 30° to 60° and then inject while withdrawing the needle. To simulate the injection scenario, we used a universal suction cup bench vise, which can be adjusted to any angle, combined with two one-dimensional sliding platforms (ODSP) with scales; ODSP 1 controls the total displacement of the injector to control the depth of injection, and ODSP 2 controls the amount of HA to be injected. On the right side of the unit, there is a mobile XY-axis device with a lifting platform, which acts as a coordinating.

2.4. System performance testing

To test the lateral resolution of the system, we stripped several carbon fibers, embedded them in heated agar and performed PAI on them after the agar had solidified. Imaging depth is an important parameter in the PAI system. To verify the imaging depth limit of the PAI system, this experiment uses an agar solution with a mass fraction of 1 % to simulate the scattering background of biological tissues. Hair strands approximately 100 μm in diameter were introduced into the simulator at an angle and then imaged in three dimensions. This experiment was designed to assess the capabilities and limitations of the PAI system in observing and probing deeper tissue structures.

2.5. PAI technology guides the syringe to the exact target area

We incubate the fertilized eggs for 15 days to allow stable blood vessels to form. Then a small piece of eggshell was gently tapped and peeled off with forceps to expose the vascular area. The syringe was inserted into the injection device and secured. The prepared embryo was placed on a lift table, raised to a certain height and secured. A few drops of water were placed on the imaging area and then PAI was performed, and the resulting blood vessel images were reconstructed in three dimensions to determine the location and spatial depth of the blood vessels. Then the knob was slowly turned to push the ODSP 1, slowly approaching the chicken embryo, according to the scale on the ODSP 1, we can see the distance of the syringe advancement in real time. When the syringe is lodged in the chicken embryo, PAI is performed again, and the relative position of the blood vessel and the syringe is obtained by 3D imaging, which allows us to visualise the angle of the syringe and whether the blood vessel will be touched during subsequent operations, and to continue advancing if the blood vessel is not touched. If there is a risk of puncturing the blood vessel, the angle of the syringe is immediately adjusted and the syringe is advanced again to ensure the integrity of the blood vessel.

2.6. Clogging of small blood vessels with HA

The vascular network on the dorsal side of the mouse tongue is essential for maintaining the normal function of the tongue tissue. Normally supplied by the large arteries, the blood vessels that enter the dorsal side of the tongue branch out into a network of smaller vessels that cover the entire dorsal region. These branching vessels are further dispersed to form a dense network on the dorsal side of the tongue. The higher density of blood vessels on the dorsal side of the mouse tongue provides sufficient oxygen and nutrients while removing metabolic waste.

The mice were anaesthetised with an intraperitoneal injection of 1 % pentobarbital sodium, the limbs and tails of the mice were then secured to a mouse board in the supine position with surgical tape, the tongue was gently pulled out with ophthalmic forceps to ensure that the mice were not injured, a resorbable suture was then threaded through the caudal end of the mice's tongue with a needle, tied in a knot and then secured to a foam plate with a syringe needle and gently tightened. The normal vasculature on the back of the mouse was first imaged as a control. The 30G syringe was then passed through the PAI system assisted injection device to insert the needle into the microvasculature and the ODSP 2 was pushed to inject approximately 5–10 μL of HA. The dorsal vessel was imaged again immediately after injection. PAI of the site was repeated at 1 day and 3 days to observe vessel occlusion.

2.7. HA clogs large blood vessels

In addition to simulating the occlusion of small blood vessels, the occlusion of large blood vessels should not be ignored. Occlusion of large blood vessels will lead directly to occlusion of blood supply, causing tissue ischaemia and necrosis, and may result in damage to the skin, subcutaneous tissue or other organs.

SD rats were anaesthetised with 1 % sodium pentobarbital by intraperitoneal injection and restrained in the supine position on a rat plate with their teeth also restrained. The rat's tongue was gently pulled out with an ophthalmic forceps in the right hand, and the blood vessels could be clearly seen, and the tongue was fixed with a needle suture in the same way as above to expose the blood vessels on the dorsum of the tongue, and then PAI was performed on the left and right vascular regions on the dorsum of the tongue to take the control blood vessel images. The location of the major blood vessels was localized by 3D imaging, and then using an assisted injection

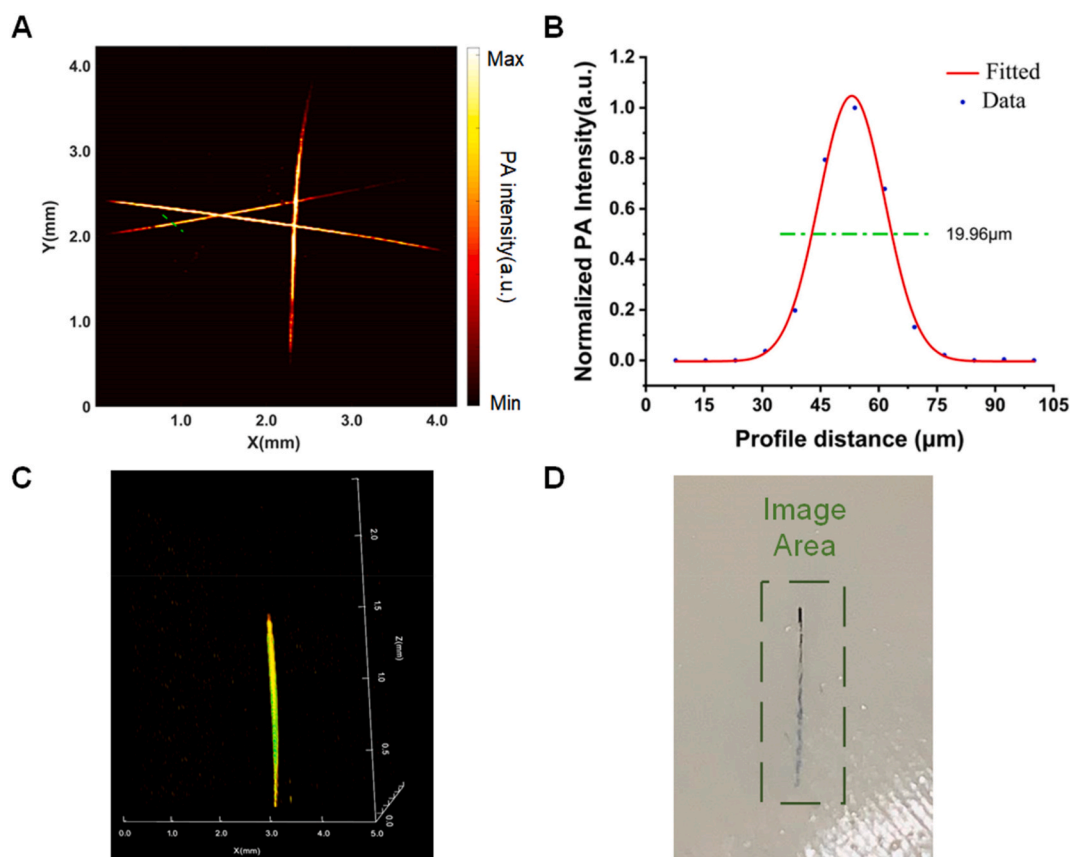


Fig. 2. PAI system performance test. (A) PAI of carbon fibers. (B) The normalized intensity of the photoacoustic signal at locations along the green line in (A). (C) Depth of PAI in the model. (D) Photograph of the sample in the agar phantom in (C). (For interpretation of the references to colour in this figure legend, the reader is referred to the Web version of this article.)

device with a 30G syringe needle, the left side of the dorsum of the tongue of the rats was injected with the major blood vessels, filled with a volume of HA of about 5–10 μL , and then the changes of vascular embolism on the left side of the dorsum of the tongue of the rats were observed by PAI at the time nodes of 0 and 1 h.

3. Results

3.1. PAI device performance

The PAI of the lateral resolution of the test system is shown in Fig. 2(A)–and a Gaussian fit was analyzed to the signal region in the drawn line part, so that we can derive the lateral resolution of the device as 19.96 μm (Fig. 2(B)). After 3D imaging of the hair strand with obliquely inserted agar (as shown in Fig. 2(C)), it can be seen that the imaging depth is about 1.5 mm, and the scanned physical image is elucidated in Fig. 2(D).

3.2. Syringe positioning

After 15 days of egg incubation, the blood vessels of the egg embryo were basically formed. From Fig. 3(A), we can clearly see two thicker blood vessels (4.8 mm in length and 0.19 mm in width) and their collateral branches, and then the depth of the blood vessels can be clearly observed in 3D imaging. After determining the spatial location of the blood vessels, we used the auxiliary injection device to simulate the injection observation. From Fig. 3(B), it can be seen that the syringe was approximately 1 mm close to the vessel, and the angle was adjusted in time to move the syringe away from the vessel on the longitudinal axis to avoid puncturing the vessel. Only in the maximum amplitude projection, as shown in Fig. 3(C), can it be seen that the needle crosses the vessel, but does not actually touch it, and a staggered distance can be observed in the later 3D figure. Fig. 3(D) then shows the result after the needle has crossed the blood vessel, in which no damage to the blood vessel can be seen even from the 2D view, and the blood vessel remains intact, fully simulating the surgical scenario of cosmetic injection of HA filler. Fig. 3(E–H) is a 3D image of the above needle reaction process. The spatial position where the blood vessels and the needle are located can be clearly seen.

3.3. Blockage of small blood vessels

The distribution of small blood vessels in the mouse tongue is dense, which can better simulate the distribution of blood vessels and veins on the surface of human skin. The untreated mouse tongue PAI results are shown in Fig. 4(A). The distribution of blood vessels and the direction of the veins in the tongue can be clearly seen and its completeness can be compared with the following experiments. Fig. 4(B) is a PAI image taken immediately after 5 μL of HA was injected at the junctions of large and small blood vessels using an auxiliary injection device. In comparison, it can be clearly seen that there are large differences before and after the injection of the

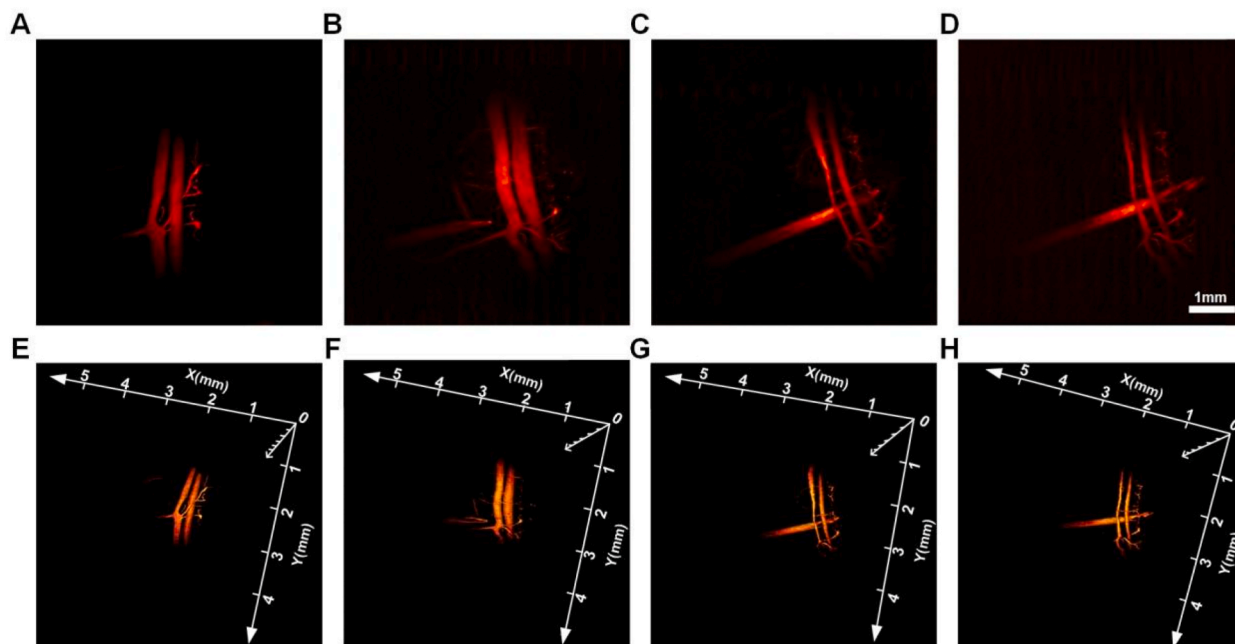


Fig. 3. PAI-guided simulation of injectable microplastics. (A) PAI of blood vessels in a chicken embryo. (B) PAI of a syringe close to a blood vessel. (C) PAI of a syringe needle passing indirectly under a blood vessel. (D) PAI of the syringe needle away from the underside of the vessel. (E–H) Corresponding 3D image to (A–D).

filler, and there is a void and weak blood signal in the blood vessels, proving that the HA has been successfully injected into the blood vessels and has blocked blood flow transport. Fig. 4(C) shows the PAI one day after HA injection. After one day of metabolism, the blood signal at the blocked site was more complete than that of the previous day, proving that the blocked blood vessel had blood transport in the restored part. Fig. 4(D) shows the PAI of the three days after injection of the HA filler. Compared with the previous

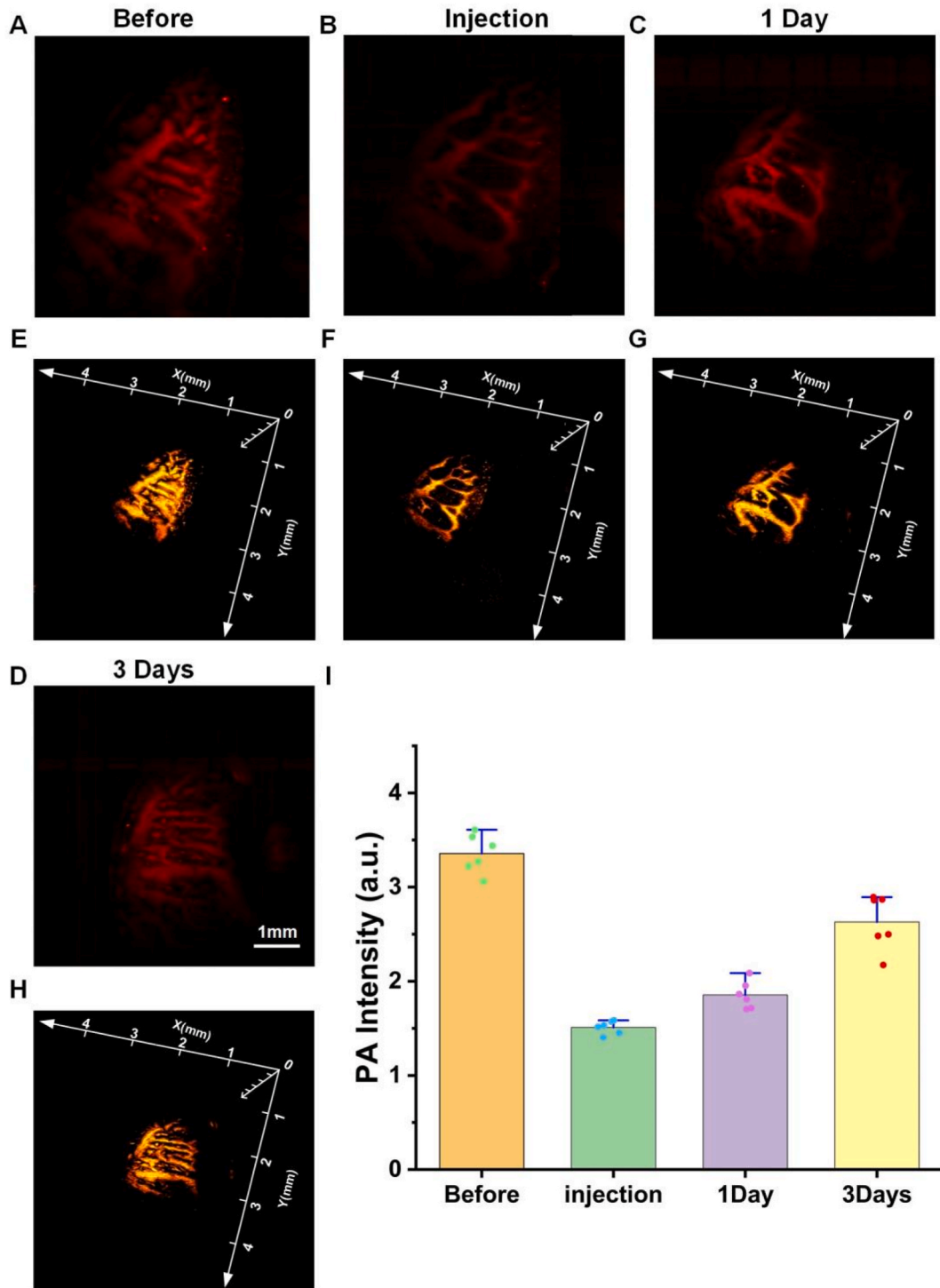


Fig. 4. Observation of HA blockade of small blood vessels and recovery. (A) PAI of tongue vessels in normal mice. (B) PAI of HA after injection into the blood vessels of the mouse tongue. (C) PAI one day after blockage of blood vessels by HA (D) PAI three days after blockage of blood vessels by HA. (E–H) Corresponding 3D images to (A–D). (I) Statistical values of vascular photoacoustic signals in (A–D).

images, the blood signal of the vein of the blood vessel is relatively complete, which proves that the blood transport of the blocked blood vessel is completely restored, and the blood flow situation is not much different from that before the injection. Fig. 4(E-H) are 3D images of the blood signals described above. The photoacoustic signal values of Fig. 4(A-D) were extracted using MATLAB (Math Works) programs, and then these data were statistically plotted using Origin, and the results are shown in Fig. 4(I) which can clearly see the trend of blood flow recovery.

3.4. Blockage of large blood vessels

For the large vessel occlusion experiments, we used the large blood vessels of the rat tongue to simulate the occlusion of the large blood vessels of the skin. As shown in Fig. 5(A), the blood vessels on the dorsal side of the rat tongue were thicker than those on the ventral side of the rat tongue, and the largest blood vessel in the field of view was up to 0.618 mm wide. 10 μ l of HA was injected into the middle of this blood vessel using the assisted injection device, and then PAI was performed again, and the results are shown in Fig. 5 (B), which showed that there was a lack of signals in the middle part of the blood vessel, demonstrating that this part of the body was filled with HA and the blood flow was blocked, resulting in incomplete blood signals. The site was imaged again 1 h later, as shown in Fig. 5(C), and comparing the images immediately after injection, it can be seen that blood flow has been restored and a more complete vascular signal is present, proving that the HA has been metabolized and there are some residuals. Fig. 5(D-F) show the 3D PAI of the three time points mentioned above, which clearly shows the blockage of the large vessel site and the restoration of blood flow.

4. Discussions

Our PAI system device uses a galvanometer scanning method to scan a 5×5 mm image in 6 s, which greatly reduces the time of conventional imaging [30,31]. In addition, it can be used to directly image the injection site in a hand-held manner, and the angle can be arbitrarily adjusted to fit the contour of the face, so that the blockage of blood vessels can be visualized by observing the change of photoacoustic signals of blood in the vessels, and the 3D imaging can also help the physician to determine the spatial location of the blockage. Although this imaging method is convenient, it sacrifices some imaging range and there is still much room for improvement when applied to the human body.

The imaging depth and resolution of the system can be further improved. The laser wavelength used in this paper is 532 nm, which is due to the high absorption characteristics of blood laser at this wavelength, but the imaging depth of the system is limited due to the strong scattering of light by biological tissue. Next, consider adding a longer wavelength laser (such as 1064 nm), using dual-wavelength or multi-wavelength imaging, to achieve greater penetration depth [32]. In addition, an ellipsoid focused ultrasonic transducer can be considered to provide high sensitivity and lateral resolution over a large depth of field to solve the problem of the

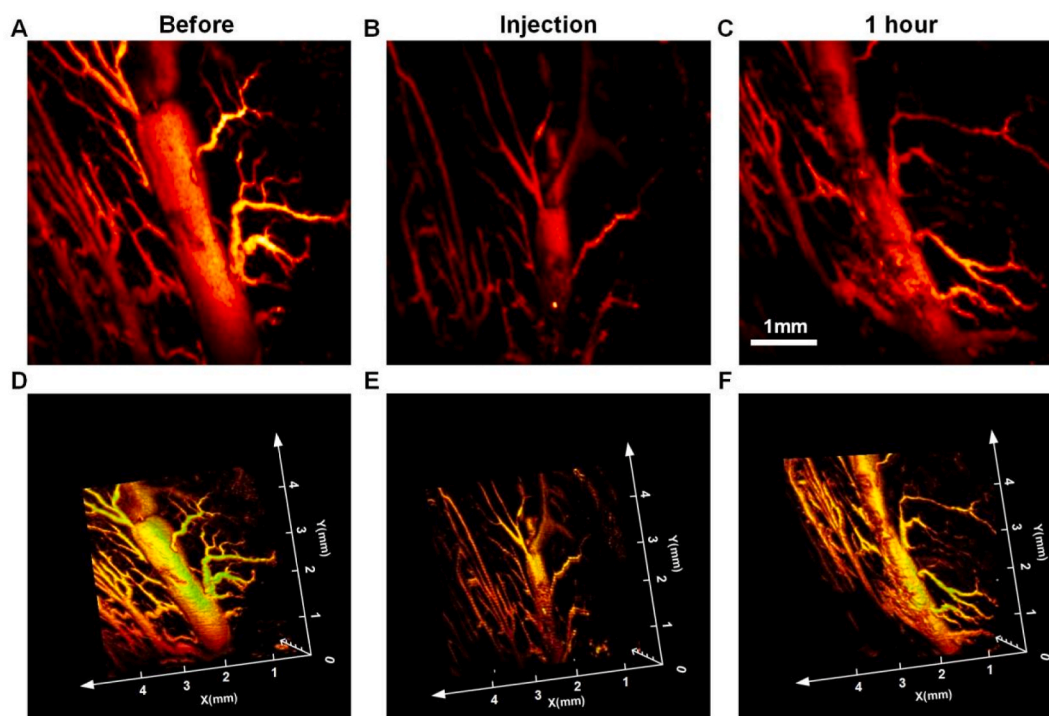


Fig. 5. Observation of HA blockade of large blood vessels and recovery. (A) PAI of blood vessels in the tongue of normal rats. (B) PAI of a large blood vessel blocked by HA. (C) PAI of a large blood vessel blocked by HA 1 h later. (D–F) Corresponding 3D images to (A–C).

rapid decline of imaging resolution with the increase of depth [33].

Since the size of the syringe needle is directly related to the damage to the biological tissue, the principle of the syringe we used is that the smaller the needle size the better, but after testing different sizes of syringes for injecting HA, we found that due to the gel-like nature of HA, it is difficult to extrude HA in the case of a small syringe size (34G syringes) and the consequence is that the syringe bursts due to the pressure and cannot be used properly. It was not possible to use it properly and eventually a suitable size (30G) was chosen. We designed an assisted injection device, guided by an optoacoustic imaging system, to obtain real-time parameters of the blood vessels around the injection area to guide the doctor to avoid dangerous blood vessels, and to adjust the angle before touching the blood vessels, and through the sliding knob and scale line, we can also reduce the human error and experience requirement of healthcare professionals, so as to achieve a precise injection amount to minimize the complication.

During the needle injection simulation, the needle of the syringe was not inserted perpendicular to the blood vessel, resulting in an angular difference, so the blood vessel was slightly squeezed, which would cause a decrease in blood flow, allowing the blood flow to be occluded and a slight deformation to occur, allowing the blood vessel become smaller. Through the occlusion experiments of different sizes of blood vessels, we found that the degradation of HA is also different, the thicker blood vessels are more difficult to completely occlude, and the blood flow is greater, and thus the thrust of the blood is greater, it is easy to metabolize most of the HA in a shorter period of time; due to the small blood vessels have less blood flow, so the degradation of HA in the small blood vessels takes longer, both of these conditions are consistent with haemodynamics.

Next, we will continue to explore the treatment of HA-clogged vessels, which clinically corresponds to immediate local injection of hyaluronidase [34–37], and some practitioners have proposed needle bleeding and extrusion in the region of the embolism, an approach that lacks experimental studies. We plan to perform 3D PAI to locate the specific site and spatial location of the blockage in different cases of vascular blockage, and then inject hyaluronidase into the inner part of the blocked blood vessel using an injection device to see if hyaluronidase can rapidly degrade HA over time compared to doing nothing, which may help guide the physician to treat the blockage symptomatically. Meanwhile, it is expected to be extended to large areas, such as application to the detection of deep blood vessels under the living body, or other micro-plastic surgery, or skin graft surgery.

Data availability statement

Data will be made available on request.

Additional information

There is no additional information available for this paper.

CRediT authorship contribution statement

Fengbing He: Writing – review & editing, Writing – original draft, Investigation, Data curation. **Xingzhi Luo:** Writing – review & editing, Writing – original draft, Investigation, Data curation. **Fan Meng:** Formal analysis. **Jiarui Chen:** Formal analysis. **Chaohao Liang:** Methodology, Investigation. **Yiqing Zhang:** Methodology, Investigation. **Shutong Liu:** Resources, Methodology. **Zishan Yuan:** Resources, Methodology. **Wuyu Zhang:** Methodology, Investigation. **Yanping He:** Resources, Project administration, Funding acquisition, Conceptualization. **Jian Zhang:** Writing – review & editing, Supervision, Resources, Project administration, Funding acquisition, Conceptualization.

Declaration of competing interest

The authors declare that they have no known competing financial interests or personal relationships that could have appeared to influence the work reported in this paper.

Acknowledgements

This study is funded by the Open Project of the Sixth Affiliated Hospital of Guangzhou Medical University (202201-210), the National Key R&D Program of China (2022YFC2304205).

References

- [1] J.A. Viscardi, C.M. Oranges, D.J. Schaefer, D.F. Kalbermatten, Reduction Mammoplasty: a Ten-Year Retrospective review of the Omega resection pattern technique, *J. Clin. Med.* 10 (19) (2021 Sep 27) 4418, <https://doi.org/10.3390/jcm10194418>.
- [2] X. Jin, M. Twayigira, W. Zhang, X. Gao, X. Luo, H. Xu, C. Huang, Y. Shen, Prevalence and associated factors of minimally invasive facial cosmetic surgery in Chinese college students, *BMC Psychiatr.* 22 (1) (2022 Jan 10) 27, <https://doi.org/10.1186/s12888-021-03676-3>.
- [3] M.H. Oley, M.C. Oley, F.O. Mawu, D.M.R. Aling, M. Faruk, Hyperbaric oxygen therapy in managing minimally invasive aesthetic procedure complications: a report of three cases, *Clin. Cosmet. Invest. Dermatol.* 15 (2022 Jan 14) 63–68, <https://doi.org/10.2147/CCID.S344408>.
- [4] M. Ramos-E-Silva, L.A. Fonteles, C.S. Lagalhard, A.P. Fucci-da-Costa, STYLAGE®: a range of hyaluronic acid dermal fillers containing mannitol. Physical properties and review of the literature, *Clin. Cosmet. Invest. Dermatol.* 6 (2013 Oct 23) 257–261, <https://doi.org/10.2147/CCID.S35251>.
- [5] F. Zheng, X. Xin, F. He, J. Liu, Y. Cui, Meta-analysis on the use of hyaluronic acid gel to prevent intrauterine adhesion after intrauterine operations, *Exp. Ther. Med.* 19 (4) (2020 Apr) 2672–2678, <https://doi.org/10.3892/etm.2020.8483>.

- [6] A. Yasin, Y. Ren, J. Li, Y. Sheng, C. Cao, K. Zhang, Advances in hyaluronic acid for biomedical applications, *Front. Bioeng. Biotechnol.* 10 (2022 Jul 4) 910290, <https://doi.org/10.3389/fbioe.2022.910290>.
- [7] K.N. How, W.H. Yap, C.L.H. Lim, B.H. Goh, Z.W. Lai, Hyaluronic acid-mediated drug delivery system targeting for inflammatory skin diseases: a mini review, *Front. Pharmacol.* 11 (2020 Jul 24) 1105, <https://doi.org/10.3389/fphar.2020.01105>.
- [8] H. Lei, C. Zhu, D. Fan, Optimization of human-like collagen composite polysaccharide hydrogel dressing preparation using response surface for burn repair, *Carbohydr. Polym.* 239 (2020 Jul 1) 116249, <https://doi.org/10.1016/j.carbpol.2020.116249>.
- [9] D. Stolic, M. Jankovic, M. Draskovic, S. Georgiev, M. Stolic, The surgical lips deformity corrected with hyaluronic fillers: a case report, *Open Access Maced J Med Sci* 3 (3) (2015 Sep 15) 423–425, <https://doi.org/10.3889/oamjms.2015.067>.
- [10] H. Zielke, L. Wölber, L. Wiest, B. Rzana, Risk profiles of different injectable fillers: results from the injectable filler safety study (IFS study), *Dermatol. Surg.* 34 (3) (2008 Mar) 326–335, <https://doi.org/10.1111/j.1524-4725.2007.34066.x>; discussion 335..
- [11] S.M. Lam, B. Azzizadeh, M. Graivier, Injectable poly-L-lactic acid (Sculptra): technical considerations in soft-tissue contouring, *Plast. Reconstr. Surg.* 118 (3 Suppl) (2006 Sep) 55S–63S, <https://doi.org/10.1097/01.prs.0000234612.20611.5a>.
- [12] M.S. Choi, S. Kwak, J. Kim, M.S. Park, S.M. Ko, T. Kim, D.S. Jeong, C.H. Rhee, G.H. Yang, W.C. Son, W.H. Kang, Comparative analyses of inflammatory response and tissue integration of 14 hyaluronic acid-based fillers in mini pigs, *Clin. Cosmet. Invest. Dermatol.* 14 (2021 Jul 2) 765–778, <https://doi.org/10.2147/CCID.S315076>.
- [13] R.M. Marticorena, S.M. Donnelly, Impact of needles in vascular access for hemodialysis, *J. Vasc. Access* 17 (Suppl 1) (2016 Mar) S32–S37, <https://doi.org/10.5301/jva.5000534>.
- [14] F. Urdiales-Gálvez, N.E. Delgado, V. Figueiredo, J.V. Lajo-Plaza, M. Mira, A. Moreno, F. Ortíz-Martí, R. Del Río-Reyes, N. Romero-Álvarez, S.R. Del Cueto, M. A. Segurado, C.V. Rebenacu, Treatment of soft tissue filler complications: expert consensus recommendations, *Aesthetic Plast. Surg.* 42 (2) (2018 Apr) 498–510, <https://doi.org/10.1007/s00266-017-1063-0>.
- [15] M. Wang, W. Li, Y. Zhang, W. Tian, H. Wang, Comparison of intra-arterial and subcutaneous testicular hyaluronidase injection treatments and the vascular complications of hyaluronic acid filler, *Dermatol. Surg.* 43 (2) (2017 Feb) 246–254, <https://doi.org/10.1097/DSS.0000000000000955>.
- [16] C. Zhang, C. Ge, C. Du, J. Li, Local cooling as a step of treatment for tissue ischemia caused by hyaluronic acid injection-induced embolism—A report of 9 cases, *Plast Reconstr Surg Glob Open* 6 (8) (2018 Aug 8) e1824, <https://doi.org/10.1097/GOX.0000000000001824>.
- [17] S. Al-Alam Sansur, D. Destang, Use of the high-dose pulsed hyaluronidase protocol in the management of impending skin necrosis associated with hyaluronic acid fillers: a systematic review, *Int. J. Oral Maxillofac. Surg.* 52 (1) (2023 Jan) 79–87, <https://doi.org/10.1016/j.ijom.2022.07.006>.
- [18] G.J. Goodman, M.R. Magnusson, P. Callan, S. Roberts, S. Hart, C.B. McDonald, M. Clague, A. Rudd, P.S. Bekhor, S. Liew, M. Molton, K. Wallace, N. Corduff, S. Arendse, S. Manoharan, A. Shamban, I. Heydenrych, A.C. Bhatia, P. Peng, T. Pavicic, K.M. Kapoor, D.E. Kosenko, A consensus on minimizing the risk of hyaluronic acid embolic visual loss and suggestions for immediate bedside management, *Aesthet Surg J* 40 (9) (2020 Aug 14) 1009–1021, <https://doi.org/10.1093/asj/sjz312>.
- [19] H. Mortada, H. Seraj, O. Barasain, B. Bamakhrama, N.I. Alhindi, K. Arab, Ocular complications post-cosmetic periocular hyaluronic acid injections: a systematic review, *Aesthetic Plast. Surg.* 46 (2) (2022 Apr) 760–773, <https://doi.org/10.1007/s00266-021-02730-5>.
- [20] W. Chen, L. Wu, X.L. Jian, B. Zhang, J.Y. Li, X.L. Qin, B. Yu, Retinal branch artery embolization following hyaluronic acid injection: a case report, *Aesthet Surg J* 36 (7) (2016 Jul) NP219–N224, <https://doi.org/10.1093/asj/sjw054>.
- [21] L. Stojanović, N. Majdić, Effectiveness and safety of hyaluronic acid fillers used to enhance overall lip fullness: a systematic review of clinical studies, *J. Cosmet. Dermatol.* 18 (2) (2019 Apr) 436–443, <https://doi.org/10.1111/jocd.12861>.
- [22] R.M. Robati, F. Moineddin, M. Almasi-Nasrabadi, The risk of skin necrosis following hyaluronic acid filler injection in patients with a history of cosmetic rhinoplasty, *Aesthet Surg J* 38 (8) (2018 Jul 13) 883–888, <https://doi.org/10.1093/asj/sjy005>.
- [23] K. Li, F. Meng, Y.R. Li, Y. Tian, H. Chen, Q. Jia, H. Cai, H.B. Jiang, Application of nonsurgical modalities in improving facial aging, *Int J Dent* (2022 Feb 24) 8332631, <https://doi.org/10.1155/2022/8332631>, 2022.
- [24] Y.A. Alharbi, Anatomical study of divergences in facial artery endings, *Anat Cell Biol* 56 (2) (2023 Jun 30) 211–218, <https://doi.org/10.5115/acb.22.262>.
- [25] G. Grigoryan, A. Sitnikov, Y. Grigoryan, Hemifacial spasm caused by the brainstem developmental venous anomaly: a case report and review of the literature, *Surg. Neurol. Int.* 11 (2020 Jun 6) 141, <https://doi.org/10.25259/SNI.56.2020>.
- [26] K.O. Tawfik, J.J. Harmon, S. Walters, R. Samy, A. de Alarcon, S.M. Stevens, T. Abruzzo, Facial palsy following embolization of a juvenile nasopharyngeal angiofibroma, *Ann. Otol. Rhinol. Laryngol.* 127 (5) (2018 May) 344–348, <https://doi.org/10.1177/0003489418761456>.
- [27] W. Zhang, H. Ma, Z. Cheng, Z. Wang, L. Zhang, K. Xiong, S. Yang, High-speed dual-view photoacoustic imaging pen, *Opt Lett.* 45 (7) (2020 Apr 1) 1599–1602, <https://doi.org/10.1364/OL.388863>.
- [28] W. Zhang, H. Ma, Z. Cheng, Z. Wang, L. Zhang, S. Yang, Miniaturized photoacoustic probe for in vivo imaging of subcutaneous microvessels within human skin, *Quant Imaging Med Surg* 9 (5) (2019) 807–814, <https://doi.org/10.21037/qims.2019.05.07>.
- [29] Laser Institute of America, American National Standard for Safe Use of Lasers ANSI Z136.1-2014, American National Standards Institute, Inc., 2014.
- [30] Y.K. Kim, C. Jung, S.J. Woo, K.H. Park, Cerebral angiographic findings of cosmetic facial filler-related ophthalmic and retinal artery occlusion, *J Korean Med Sci* 30 (12) (2015 Dec) 1847–1855, <https://doi.org/10.3346/jkms.2015.30.12.1847>.
- [31] W. Lee, J.S. Kim, H.J. Moon, E.J. Yang, A safe Doppler ultrasound-guided method for nasolabial fold correction with hyaluronic acid filler, *Aesthet Surg J* 41 (6) (2021 May 18) NP486–NP492, <https://doi.org/10.1093/asj/sjaa153>.
- [32] Wang, Z, Yang, F, Ma, H, Cheng, Z, Zhang, W, Xiong, K, Shen, T, Yang, S. Bifocal 532/1064 nm alternately illuminated photoacoustic microscopy for capturing deep vascular morphology in human skin. *J. Eur. Acad. Dermatol. Venereol.* : JEADV, 36(1), 51–59, <https://doi.org/10.1111/jdv.17677>.
- [33] D. Zhang, Z. Wang, Z. Cheng, W. Zhang, F. Yang, S. Yang, An ellipsoidal focused ultrasound transducer for extend-focus photoacoustic microscopy, *IEEE (Inst. Electr. Electron. Eng.) Trans. Biomed. Eng.* 68 (12) (2021) 3748–3752, <https://doi.org/10.1109/TBME.2021.3078729>.
- [34] W. Thanasarnakorn, S. Cotofana, C. Rudolph, P. Kraissak, N. Chanasumon, A. Suwanachinda, Severe vision loss caused by cosmetic filler augmentation: case series with review of cause and therapy, *J. Cosmet. Dermatol.* 17 (5) (2018 Oct) 712–718, <https://doi.org/10.1111/jocd.12705>.
- [35] C. Zheng, Q. Fu, G.W. Zhou, L.Y. Lai, L.X. Zhang, D.Q. Zhang, G.J. Chen, L.M. Liang, M.L. Chen, Efficacy of percutaneous intraarterial facial/supratrochlear arterial hyaluronidase injection for treatment of vascular embolism resulting from hyaluronic acid filler cosmetic injection, *Aesthet Surg J* 42 (6) (2022 May 18) 649–655, <https://doi.org/10.1093/asj/sjab425>.
- [36] L. Zhang, L. Pan, H. Xu, S. Yan, Y. Sun, W.T.L. Wu, S. Wu, Clinical observations and the anatomical basis of blindness after facial hyaluronic acid injection, *Aesthetic Plast. Surg.* 43 (4) (2019 Aug) 1054–1060, <https://doi.org/10.1007/s00266-019-01374-w>.
- [37] L. Zhang, Z. Luo, J. Li, Z. Liu, H. Xu, M. Wu, S. Wu, Endovascular hyaluronidase application through superselective angiography to rescue blindness caused by hyaluronic acid injection, *Aesthet Surg J* 41 (3) (2021 Feb 12) 344–355, <https://doi.org/10.1093/asj/sjaa036>.